IOP Publishing and International Atomic Energy Agency Nuclear Fusion
Nucl. Fusion **50** (2010) 105010 (8pp) doi:10.1088/0029-5515/50/10/105010

Strike point control for the National Spherical Torus Experiment (NSTX)

E. Kolemen[1], D.A. Gates[1], C.W. Rowley[2], N.J. Kasdin[2], J. Kallman[1], S. Gerhardt[1], V. Soukhanovskii[1] and D. Mueller[1]

[1] Princeton Plasma Physics Laboratory, Princeton, NJ 08543, USA
[2] Mechanical and Aerospace Engineering, Princeton University, Princeton, NJ 08544, USA

Received 4 March 2010, accepted for publication 8 July 2010
Published 1 September 2010
Online at stacks.iop.org/NF/50/105010

Abstract
This paper presents the first control algorithm for the inner- and outer-strike point position for a Spherical Torus (ST) fusion experiment and the performance analysis of the controller. A liquid lithium divertor (LLD) will be installed on NSTX which is believed to provide better pumping than lithium coatings on carbon PFCs. The shape of the plasma dictates the pumping rate of the lithium by channelling the plasma to LLD, where the strike point location is the most important shape parameter. Simulations show that the density reduction depends on the proximity of the strike point to LLD. Experiments were performed to study the dynamics of the strike point, design a new controller to change the location of the strike point to the desired location and stabilize it. The most effective poloidal field (PF) coils in changing inner- and outer-strike points were identified using equilibrium code. The PF coil inputs were changed in a step fashion between various set points and the step response of the strike point position was obtained. From the analysis of the step responses, proportional–integral–derivative controllers for the strike points were obtained and the controller was tuned experimentally for better performance. The strike controller was extended to include the outer-strike point on the inner plate to accommodate the desired low outer-strike points for the experiment with the aim of achieving 'snowflake' divertor configuration in NSTX.

(Some figures in this article are in colour only in the electronic version)

1. NSTX strike point control for LLD

1.1. LLD installation at NSTX

In order to improve the performance of the confined plasma and to better control the core plasma density, the National Spherical Torus Experiment (NSTX, $R = 0.85\,\mathrm{m}, a < 0.67\,\mathrm{m}$, $R/a > 1.27$) [1] has been investigating the use of lithium as a surface coating material. To reach this aim, NSTX has been installed with an evaporative lithium system (LiThium EvaporatoR or LiTER) to coat the graphite tiles that cover the inner walls [2]. This led to 50% reductions in L-mode density and 15% reductions in H-mode [3]. The introduction of a second evaporator in 2008 improved energy confinement times ($\tau_E > 100\,\mathrm{ms}$) and pulse lengths (1.8 s), and reduced edge localized mode activity [4]. Currently, the liquid lithium divertor (LLD) is being installed at NSTX in order to overcome the continuous increase in the core density during the shots. LLD is a thick, toroidally continuous liquid lithium surface, which will absorb a significant particle flux (see figure 1). The LLD is a joint collaboration between Sandia National Laboratory, University of California at San Diego and the NSTX project.

1.2. Importance of strike point control for NSTX operation with LLD

The particles that hit the NSTX wall dominantly follow the last closed flux surface and thus land near the outer-strike point, the location on the wall that has the same magnetic flux as the last closed flux surface. Employing the multi-fluid code UEDGE edge numerical plasma transport simulation code, Stotler *et al* [5] studied the effect of the reduced recycling that is provided by the LLD module. Their results show that density reduction depends on the proximity of the outer-strike point to LLD. In addition, the strike point must avoid hitting the coaxial helicity injection (CHI) gap [6], since this may induce a disruption of the plasma. Finally, it is important to control the gap between the strike point and LLD since the heat flux is very highly concentrated near the strike point, and this heat may be damaging to the LLD structure. Thus, in order to obtain better and more consistent density reduction and to avoid contact with the LLD and the CHI gap, the strike point position is of critical importance. With this motivation, we started the development and implementation of the strike point control algorithm.

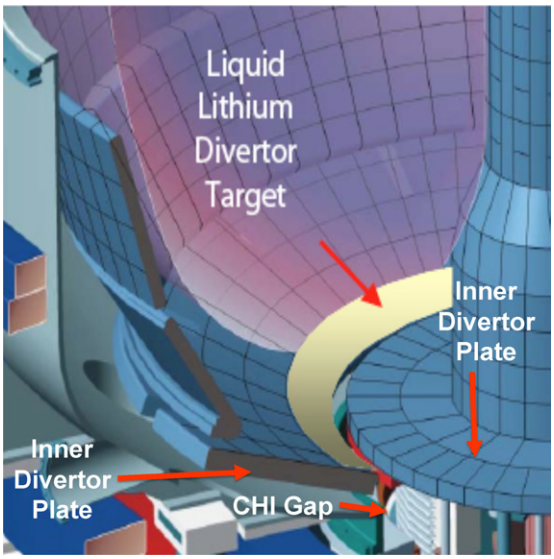

Figure 1. Illustration of the LLD in the NSTX.

2. Preliminary studies of strike point dynamics

2.1. Analysis of the strike point motion via ISOLVER

To gain insight into strike point control, we carried out preliminary studies using ISOLVER. ISOLVER is a predictive free-boundary auto-convergent axisymmetric equilibrium solver developed by Huang and Menard [7]. This software takes the normalized pressure, current profiles and boundary shape as input, after which it matches a specified plasma current and β and computes coil currents as its output. Alternatively, the coil currents can be specified as the input and the boundary shape as output.

First, we tried to determine which poloidal field (PF) coil(s) should be used for outer-strike point control. Currently at NSTX, PF3L is used for vertical stability control. This leaves PF1AL, PF1BL and PF2L as the available control inputs. ISOLVER simulations showed that, due to its proximity to the desired radial outer-strike point location, $r_{\text{st-o}}$, PF2L is two to three times more effective than the alternative coils. Thus, PF2L was chosen as the sole controller for the outer-strike point. We then started to analyse the single input single output model (SISO) from PF2L current to the outer-strike point position.

2.2. First-order-plus-dead-time (FOPDT) model for SISO

Analysing the effect of PF2L on the outer-strike point location, we gained two important insights. First, ISOLVER analysis showed that the input/output system is linear in the region of interest as shown in figure 2 and roughly a 1 kA change in PF2L current leads to a change of 5 cm in radial outer-strike point location. Thus, it is reasonable to model its dynamics as a linear ordinary differential equation of which the first-order form is the simplest one to adopt.

Second, there are delays from the request of control input to action in the system. Most importantly, the real time EFIT (EFITRT) [8] calculations take a few milliseconds. In order to control the strike point, we must first calculate its location,

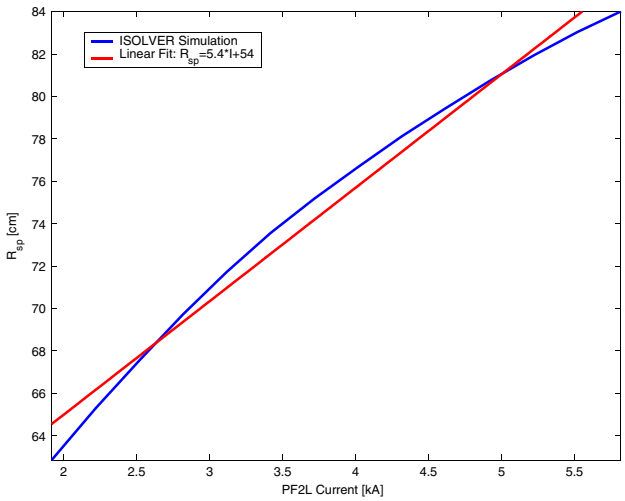

Figure 2. Relationship between the radial strike point position and the PF2L current.

which means that we must wait until the data from EFITRT are available.

We concluded that, for the purpose of control design, the simplest model for the SISO dynamics (PF2L current to Strike Point change) is a FOPDT model, which would be representative of the real system dynamics. In the time domain, the FOPDT is written as

$$\dot{y}(t) = -\frac{y(t) + Ku(t - L)}{T} \tag{1}$$

or, in the more commonly used form in the Laplace domain, the transfer function, G, from the control, u, to output, y, is

$$\mathrm{G}(s) = \frac{y(s)}{u(s)} = \frac{K}{1 + sT}\mathrm{e}^{-sL}. \tag{2}$$

FOPDT is defined in terms of three parameters: the static gain K, the time constant T and the dead time L. This is the most commonly used process model in proportional–integral–derivative (PID) controller tuning.

3. System identification experiment

In order to control a system of interest, we must first identify the internal dynamics of that system. This process is called system identification. In our case this entailed estimating the parameters K, T and L of the FOPDT model.

We designed an experiment to find these parameters from the process reaction curve (PRC), which is the open-loop output response of a process to a step change in the input (see [9] and references therein). This commonly used system identification method is based on the time domain response of the system. The step response of the FOPDT model given in equation (2) is

$$\begin{aligned} \Delta y(t) &= K\left(1 - \mathrm{e}^{-(t-L)/T)}\right)\Delta u; & t > L \\ &= 0; & t \leqslant L. \end{aligned} \tag{3}$$

In the system identification experiment, we introduced perturbations in the PF2L requests and measured the strike point response. From the experimentally obtained PRC, the three parameters are found by curve fitting.

Table 1. Experiment setup: initial $r_{\text{st-o}}$, PF2L step input and the estimated variation in $r_{\text{st-o}}$.

Shot number	132185	132186	132187	132188	132190	132192	132193	132198	132199	132200
Initial $r_{\text{st-o}}$ (cm)	70	70	70	70	71	71	70	62	64	63
ΔI_{PF2L} (kA)	0	1	1	0.5	−0.4	−0.5	−1	1	2	0
Estimated $\Delta r_{\text{st-o}}$ (cm)	0	5	5	2.5	−2	−2.5	−5	5	10	0

3.1. Experiment steps

The experiment consisted of the following steps:

(1) We began with a well performing shot (shot # 120001) and obtained the plasma shape of approximately lower triangularity = 0.55, upper triangularity = 0.35, average triangularity = 0.45, elongation = 2.3.
(2) We stabilized the plasma for this shape.
(3) From the previously defined strike point versus PF2L coil current curves, we set the PF2L coil current in a step way to obtain the changes in $r_{\text{st-o}}$ in the range from 60 to 80 cm.

Table 1 shows the successful experimental shots. The first and last shots were designated as the baseline shots, with no change in the current request, to which all the remaining shots were compared. In order to get a broader range, the first seven shots were taken with $r_{\text{st-o}}$ of roughly 70 cm and the last three of roughly 63 cm. Different steps in the positive and negative direction were taken to get a range $\Delta r_{\text{st-o}}$ of −5 to 10 cm. The PF2L coil current to induce these for the I_{i} of these shots ranges between 0 and 20 kA.

3.2. Experiment analysis

NSTX uses the Plasma Control System (PCS) developed by General Atomics which 'is a software application used to monitor and control various attributes of plasmas generated for fusion research including plasma shape, position, electron temperature at a specific radial location, density and rotation' [10]. The shape control algorithm in this software architecture is defined in terms of the polodial fluxes and has been successfully used for boundary control [11, 12]. In other words, to be compatible with PCS, $y(t)$ in equation (3) should be defined in terms of polodial flux at the strike point as opposed to strike point location.

Figure 3 shows the results of the experimental shots [132185, 132186, 132187, 132188, 132189, 132190, 132191, 132192, 132193, 132198, 132199, 132200]. In the figure, the x-axis is the time and the y-axis is the $y(t)/u(t)$ resulting from the start of the step response. As discussed above, $y(t)$ is the polodial flux and $u(t)$ is the PF2L current. The blue lines show the results from different experiments, the red line is the average of all these experiments.

We found the parameters from the average response curve. The static gain, $K = \Delta y_{\text{ss}}/\Delta u$, or the ratio of the steady state output, Δy_{ss}, to input, Δu, is read off the plot as 2.36×10^{-6} (Wb rad^{-1}) A^{-1}. In order to find the time constant T and the dead time L, we need to find the FOPDT model, given in equation (3), that best fits the PRC. Many curve-fitting methods have been developed specifically for this purpose, of which the tangent and two point methods are the most prominent (see Gopal *et al* [13] for detailed information about these methods). We used these two methods. The tangent method gave the $T = 7.0$ ms and $L = 6.6$ ms, while the two points method

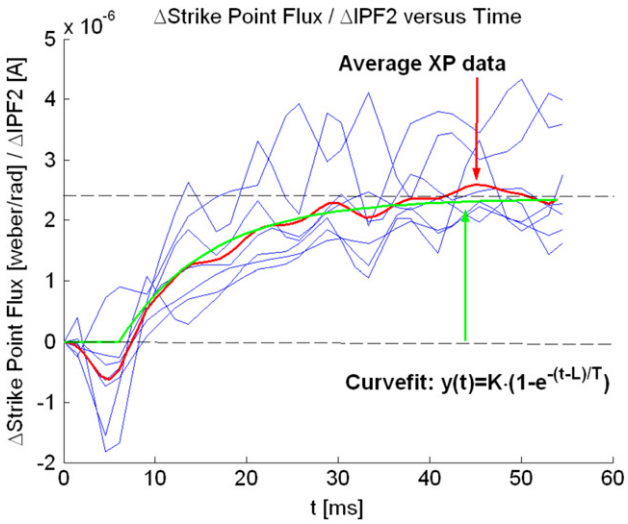

Figure 3. System identification experimental data and FOPDT curvefit.

gave $T = 12.9$ and $L = 5.5$ ms. Taking the average, from here on we assume the following: $T = 9.95 \pm 3.0$ ms and $L = 6.05 \pm 0.6$ ms. The FOPDT model with these parameters is plotted as the green line in figure 3, which shows a reasonable fit with experimental data.

4. A proportional–integral–derivative (PID) controller for the outer-strike point

Currently, the PCS only accepts controllers of the PID type. As a result, we designed a PID controller for the strike point control.

A PID controller is a generic control loop feedback mechanism which attempts to minimize the error between a measured process variable and a desired setpoint via a corrective action. A general PID controller can be written in the standard form as

$$u(t) = K_{\text{p}}\left(e(t) + \frac{1}{T_{\text{i}}}\int_0^t e(\tau)\,\mathrm{d}\tau + T_{\text{d}}\frac{\mathrm{d}}{\mathrm{d}t}e(t)\right), \qquad (4)$$

where

$$e(t) = r(t) - y(t), \qquad (5)$$

and $r(t)$ is the reference signal (set point) and $y(t)$ corresponds to the measured polodial magnetic flux at the requested outer-strike point location. In this form, the K_{p} gain is applied to integral and derivative terms, where T_{i} is the integral time and T_{d} is the derivative time.

In the ideal parallel form shown in figure 4, the gain parameters are related to the parameters of the standard form through the relationship $K_{\text{i}} = K_{\text{p}}/T_{\text{i}}$ and $K_{\text{d}} = K_{\text{p}}T_{\text{d}}$.

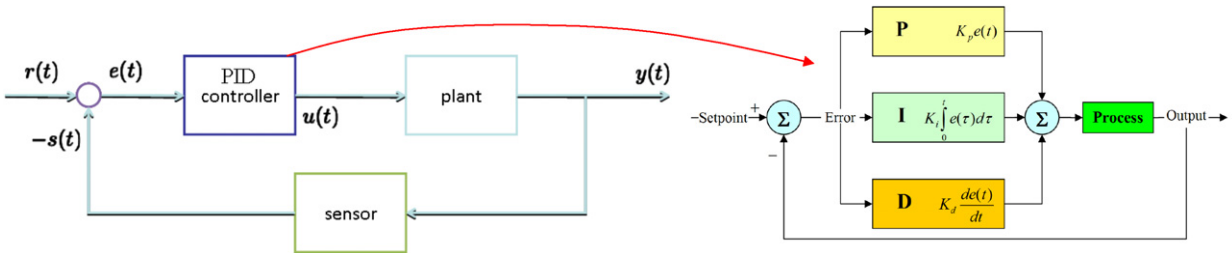

Figure 4. Block diagram of a PID.

Table 2. Ziegler and Nichols PID controller gains.

Controller type	K_p	T_i	T_d
P	$\frac{1}{K}\frac{T}{L}$	—	—
PI	$\frac{0.9}{K}\frac{T}{L}$	$3.33L$	—
PID	$\frac{1.2}{K}\frac{T}{L}$	$2.0L$	$0.5L$

4.1. PID tuning

The tuning of a PID loop involves setting the three gain coefficients in order to calibrate how vigorously the controller reacts to errors between the measured process variable and the desired setpoint. If the control is too aggressive, the controller may react excessively to small disturbances, which leads to instability. On the other hand, a sluggish controller performs poorly, leading to a very long time to reach the setpoint.

There are various tuning algorithms, each of which performs better in a different parameter range of dynamical systems. An important indicator for choosing the best tuning algorithm for the dynamical system under consideration is the parameter $\tau = L/(T + L)$, which in our case is equal to 0.38. On page 232, Xue *et al* [14] show that for FOPDT systems with τ in the range $0.16 < \tau < 0.57$, the regular Ziegler and Nichols algorithm gives the best control performance. Thus, we use this well-known heuristic algorithm, which was developed by Ziegler and Nichols and based on many years of experience in controls. This tuning law, shown in table 2, gives the PID coefficients from the three parameters that we identified in the last section.

4.2. PID coefficients from the experiment

On page 109, Astrom *et al* [9] show that processes of a predominantly first-order character with parameters within our range are controllable satisfactorily with a PI only controller, even though the addition of the derivative term increases performance. The derivative part of a PID uses the rate at which the system moves to control the process. To include the derivative term without causing performance degradation, we need either a relatively smooth process or a filter that can smooth out the jitter in the measurements while maintaining the trend data. However, even though the real strike motion of the plasma does not generally move abruptly, the measured strike point location sometimes does, due to the reconstruction of the EFITRT. To avoid such problems with reconstruction, we avoided the use of the derivative of the measured data in the control algorithm, and opted for PI only control.

$$I(t) = K_p\left(e(t) + \frac{1}{T_i}\int_0^t e(\tau)\,d\tau\right). \tag{6}$$

Employing the Ziegler and Nichols method given in table 2, we obtained $K_p = 6.27 \times 10^5$ A/(Wb rad^{-1}) and $T_i = 0.018$ s from the PF2L current input to the outer-strike point polodial flux.

In PCS, the control input is the voltage request as opposed to the current request. To find the PI controller for the system with voltage as the input, we first write the current and voltage relationship given as

$$R\,I(t) + L_{ind}\frac{dI}{dt}(t) + \frac{1}{C}\int_{-\infty}^{t} I(\tau)\,d\tau = v(t). \tag{7}$$

For the PF2L coil, we can ignore the capacitance. The inductance is $L_{ind} = 1.98 \times 10^{-3}$ H (note that we are using the notation L_{ind} to differentiate between the time lag, L and inductance) and the resistance is $R = 4.17 \times 10^{-3}\,\Omega$. Substituting equation (6) in equation (7), we can write voltage in terms of the flux error as

$$v(t) = \left(RK_p + \frac{L_{ind}K_p}{T_i}\right)\left\{e(t) + \frac{R/T_i}{R + (L_{ind}/T_i)}\int_0^t e(\tau)d\tau\right\}, \tag{8}$$

where the derivative terms are ignored. Thus,

$$K_{p\,volt} = RK_p + \frac{L_{ind}K_p}{T_i} \quad \text{and}$$

$$T_{i\,volt} = \frac{R + (L_{ind}/T_i)}{R/T_i} = T_i + \frac{L_{ind}}{R}. \tag{9}$$

Finally, taking into account that PCS has a multiplicative factor of 200 between the requested voltage by the software and the voltage request sent to the PF coils, we obtain $K_{p\,volt} = 356 \pm 170$ A/(Wb rad^{-1})*H/s = V/(Wb rad^{-1}) and $T_{i\,volt} = 0.493 \pm 0.002$ s (or $K_i = 722 \pm 345$). Note that $T_{i\,volt} \approx L_{ind}/R$ is almost independent of any other parameter due to the low value of lag in the NSTX PCS, which is in the order of a few milliseconds and thus $T_i \ll L_{ind}/R$. We expect this result relationship to hold for other PF coils as well; this may be useful in future control designs.

5. Testing and tuning the PID controller for the strike point

After the nominal PI gains were obtained, we tested the controller. Table 3 shows the PI controllers tested in the second part of the experiment.

Table 3. Tested K_p and K_i values in the experiment.

Shot number	133878	133879	133880	133884	133885	133886	133887	133888
K_p	550	275	275	275	400	400	500	400
K_i	0	0	200	400	600	800	1000	800

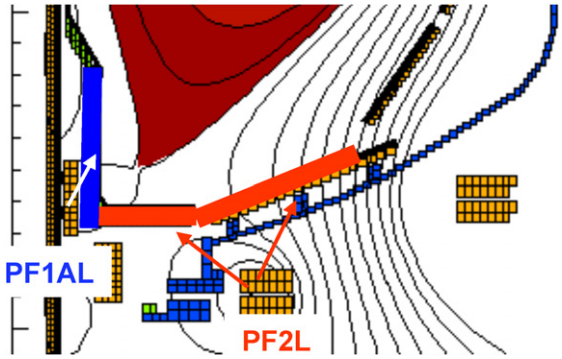

Figure 5. Control segments for the inner-strike point on the vertical plate via PF1AL and the outer-strike point on the inner and outer plates via PF2L.

The PI controller with K_p of 500 was unstable. The shot numbered 133886 gave the best performance. Shot 133888 was repeated to confirm that the results were consistent. Thus, the PI gains were set to $K_p = 400$ and $K_i = 800$, which correspond closely to the predicted values from the system identification and Ziegler and Nichols gain tuning.

6. Extensions to control: inner-strike point control and outer-strike point control on the inner divertor plate

6.1. Inner-strike point

After achieving a satisfactory control using the outer-strike point controller, we used it for an experiment which investigated the intermediate triangularity discharge with lithium PFC coatings. While the controller kept $r_{st\text{-}o}$ at the requested position, there were problems during the transient phase of the discharge. The equilibrium bifurcated to two solutions: the desired configuration with medium X-point and the inner-strike point on the vertical plate, and a configuration with a very low X-point and the inner-strike point on the inner divertor plate. The solution oscillated between the two nearby equilibria. This led to the plasma scraping the lower tiles. To keep the plasma in the desired configuration and make it more stable, we added an inner-strike point controller. Figure 5 shows the added inner strike point control segment on the horizontal plate where the height of the strike point, $z_{st\text{-}i}$, is the control objective. PF1AL is very close to this control segment and the most effective coil to control $z_{st\text{-}i}$. As a result, it was used as the sole control input for the inner-strike point control.

The inner-strike point was not as crucial a parameter to control as the outer-strike point for the operation of NSTX with LLD. A coarser control was considered adequate for $z_{st\text{-}i}$. Thus, we skipped the system identification and started the manual PI controller tuning directly. We started with smaller gains and increased them until the control was satisfactory. Table 4 shows the PI parameters that were tried during the experiment. Gain values of K_p and K_i of 5000 were found to be acceptable and used for $z_{st\text{-}i}$ control.

Table 4. PI tuning experiment for inner-strike point control.

Shot number	134970	134974	134976	134977	134978	134986	134987
K_p	100	300	400	800	1600	5000	5000
K_i	700	2100	3500	6000	12000	5000	5000

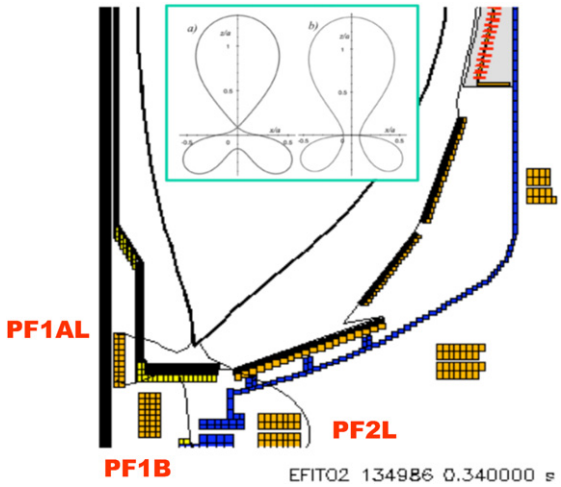

Figure 6. An example snowflake-plus configuration achieved on NSTX. Illustrated on top are (*a*) the theoretical snowflake-plus and (*b*) snowflake-minus configurations.

Table 5. Outer-strike point scan for snowflake configuration experiment.

Shot number	135478	135480	135481	135484	135485	135486
$r_{st\text{-}o}$ [cm]	44	48	50	55	55	73

6.2. Extended outer-strike point on the inner plate and the 'snowflake' divertor configuration

The 'snowflake' divertor configuration is a second-order polodial field null, i.e. the first derivatives of the magnetic field, B_p, also vanish at the null point and the separatrix divides the poloidal plane into six sectors, created in the divertor region by placing two X-points in close proximity to each other. In the vicinity of the second-order null poloidal B_p increases with the square of the distance form the divertor where as in a regular first-order X-point B_p increases linearly in distance. Snowflake configuration thus has higher divertor flux expansion due to the lower B_p throughout the divertor region. Also, snowflake configuration has different edge turbulence and magnetic shear properties. These properties are beneficial for divertor heat flux reduction, and turbulence

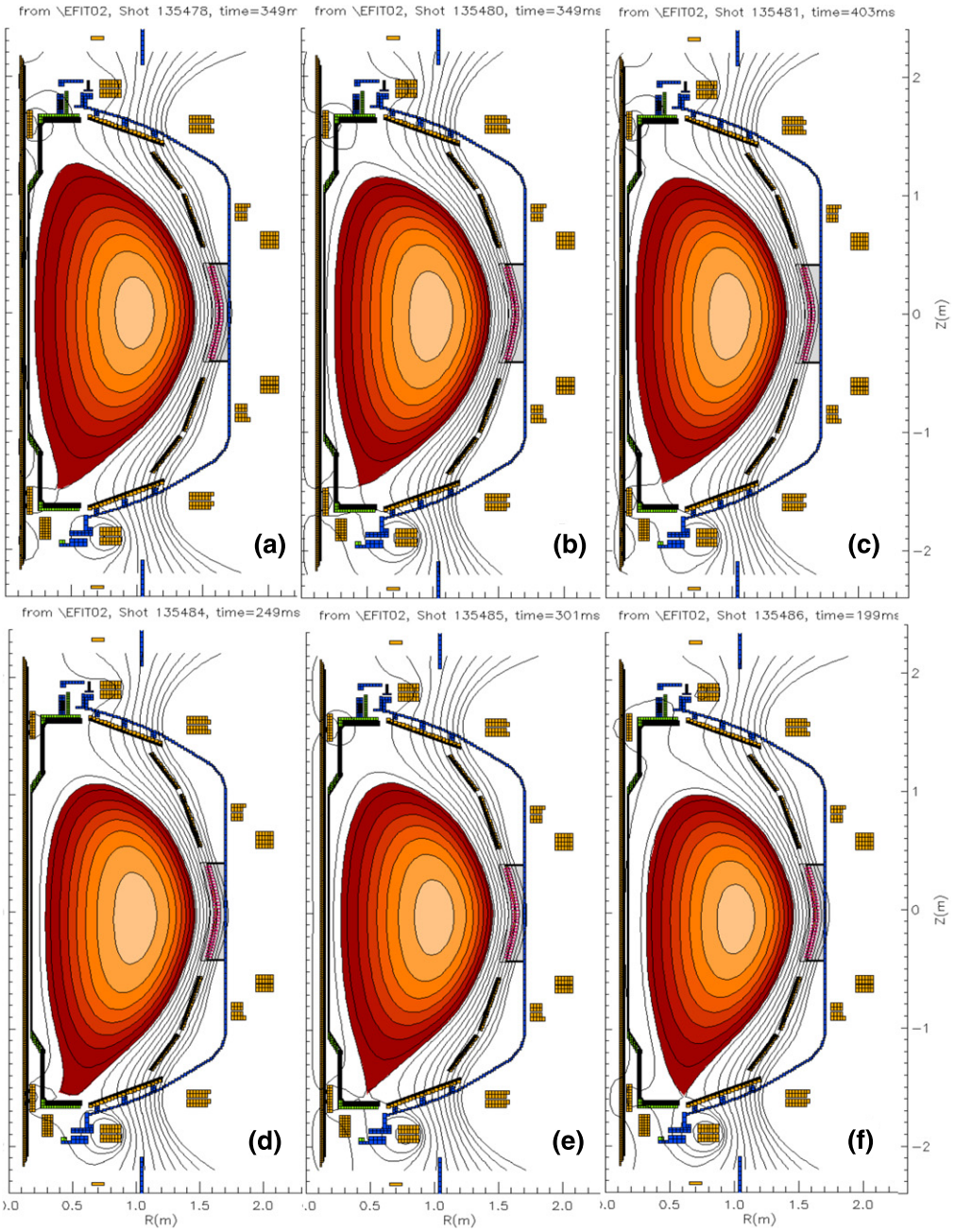

Figure 7. Snap shots from the snowflake scan experiments. The request for the outer-strike point positions from (*a*) to (*f*) are 44 cm, 48 cm, 50 cm, 55 cm, 55 cm, 73 cm, respectively. There is no snowflake in (*a*). Snap shot times are chosen to illustrate configurations which are close to the snowflake.

and ELM control. Since the snowflake configuration is an unstable configuration, in experiments nominally slightly perturbed version of the theoretical configurations called snowflake-minus and snowflake-plus are achieved [15]. These configurations and an example from NSTX are shown in figure 6. For more information on the snowflake concept, see [16, 17].

We implemented and used the combined inner/outer-strike point control to test the snowflake configuration. The snowflake configuration usually occurs with smaller $r_{\text{st-o}}$. In order to obtain this smaller $r_{\text{st-o}}$, we extended the outer-strike point controller to the inner divertor plate as shown in figure 5. This work was performed to support an experiment designed to investigate the viability of maintaining a snowflake divertor in NSTX.

The aim of the experiment was to investigate if snowflake configuration was achievable in NSTX and if so to roughly identify the region in phase space of the possible parameters. In the experiment, we used both the inner- and outer-strike point controller to achieve a snowflake configuration. The parameter that effects B_{p} around the X-point is the outer-strike point. Thus in the experiments we scanned the outer-strike point from 44 to 73 cm. Table 5 shows the shot numbers and the $r_{\text{st-o}}$ requests used in this experiment. Figure 7 shows samples from the series of experiments. In each of these shots, $r_{\text{st-o}}$ and $z_{\text{st-i}}$ were fixed. The two other controllable shape parameters

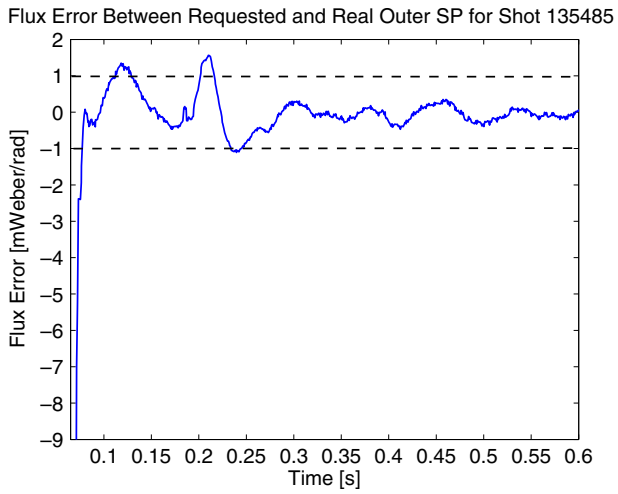

Figure 8. Flux error between the achieved and the desired strike point locations.

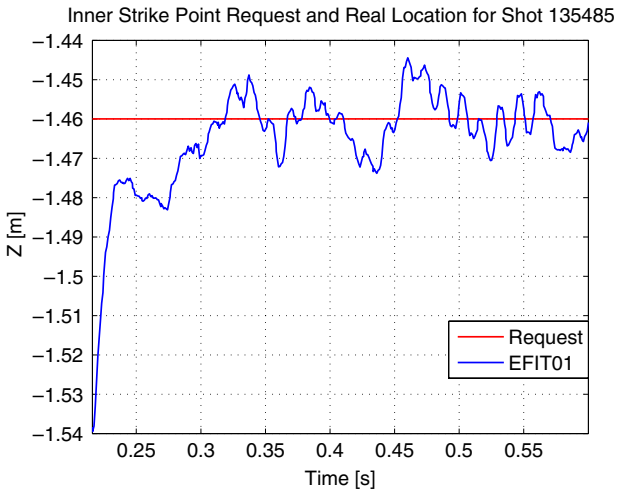

Figure 9. Control of the inner-strike point on the horizontal plate.

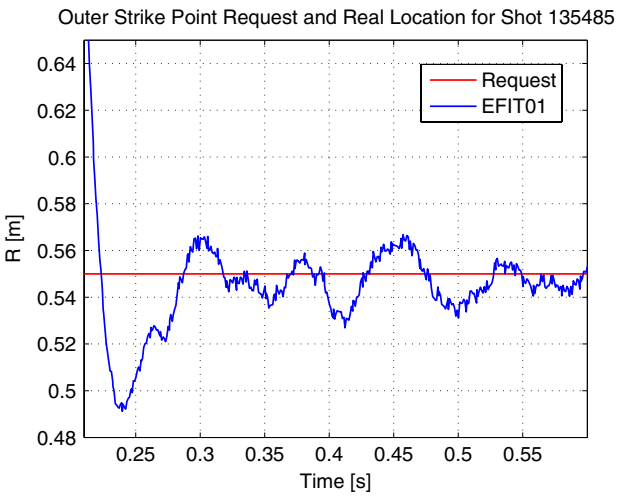

Figure 10. Control of the outer-strike point position on the inner plate.

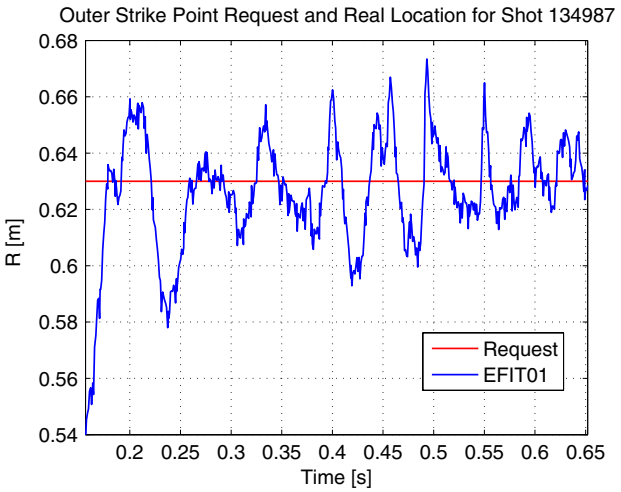

Figure 11. Control of the outer-strike point on the outer plate.

that have a noticeable effect on B_p around the X-point are squareness, ζ, and $\Delta_{r_{sep}}$. Squareness is a shape parameter that defines how similar the boundary of the plasma is to a square, such that a triangle has $\zeta = 0$ and a rectangle has $\zeta = 1.0$. $\Delta_{r_{sep}}$ is equal to $[R(\psi(X_1) - R(\psi(X_2)]|_{z=0, R>R_0}$, where the notation X_1 is used for lower X-point, $X_1 = [R, Z]_{\text{X-point}_1}$, and X_2 is used for upper X-point, $X_2 = [R, Z]_{\text{X-point}_2}$. In order to push the two X-points closer to each other, these two free control parameters were varied in a gradient search fashion, i.e. increase the magnitude if we are approaching and decrease otherwise. As a result, we were able to achieve transient snowflake configurations with $r_{\text{st-o}}$ from 48 to 73 cm and identified that the longest and most stable configuration is around $r_{\text{st-o}}$ 55 cm.

7. Results and performance of the strike point controller

As shown in figure 5, the controllers were used for the inner-strike point on the vertical plate, and for the outer-strike point on the inner horizontal plate and on the outer plate.

The outer- and inner-strike point controllers achieved <1 mW rad^{-1} error in the polodial flux, as shown in an example shot in figure 8. These errors correspond roughly to root mean square (RMS) values of <1 cm error in $r_{\text{st-i}}$, <1.5 cm error in $r_{\text{st-o}}$ on the inner divertor and <2 cm error in $r_{\text{st-i}}$ on the outer divertor, as shown in figures 9, 10 and 11, respectively. The finely tuned controllers performed satisfactorily without becoming unstable. An important requirement for the generic NSTX strike point controller was that it should be able to work smoothly with very different starting plasma conditions and corresponding strike point locations. The controllers were capable of handling large initial errors.

The outer-strike point controller with a RMS value of <2 cm error gives enough accuracy to commission and test the LLD for NSTX. This accuracy is enough to move the strike point close but not on top of the LLD and to observe the change in the density of the plasma with a variation in the strike point location. A more detailed study will probably need higher accuracy. As part of future work, we intend to extend the

PI controllers to PID. Adding a derivative term should reduce the RMS error. Also, the current method we used tuned the PF2L coil gains without taking into account the effect of the PF1AL controller and vice versa for PF1AL. Retuning the coils by taking into account the mutual effect should enhance the control performance.

8. Summary

This paper presented the new control algorithm for the inner- and outer-strike point position for NSTX and the performance analysis of the controller. A LLD will be installed on NSTX which provides better pumping than lithium coatings on carbon PFCs. In order to obtain better and more consistent density reduction and to avoid contact with the LLD and the CHI gap, strike point controllers were developed. The controllers were tested and tuned to achieve stabilization of the strike points to within <1 mW rad^{-1} in polodial flux error, which corresponds to roughly <1 cm in position error. These controllers will be used in regular operation of NSTX when LLD is installed. Strike point controllers also enable consistent and stable operations under previously unachievable configurations, such as the snowflake configurations.

Acknowledgments

This work was supported by the US Department of Energy Grant under contract number DE-AC02-76CH03073.

References

[1] Ono M. *et al* and NSTX Team 2000 Exploration of spherical torus physics in the NSTX device *Nucl. Fusion* **40** 557–61

[2] Kugel H.W. *et al* 2007 Effect of lithium PFC coatings on NSTX density control *J. Nucl. Mater.* **363–365** 791–6 (Plasma–Surface Interactions-17)

[3] Kugel H.W. *et al* 2008 The effect of lithium surface coatings on plasma performance in the National Spherical Torus Experiment *Phys. Plasmas* **15** 056118

[4] Kugel H.W. *et al* 2009 Evaporated lithium surface coatings in NSTX *J. Nucl. Mater.* **390–391** 1000–4

[5] Stotler D.P., Maingi R., Kugel H.W., Pigarov A.Yu., Rognlien T.D. and Soukhanovskii V.A. 2010 Simulations of NSTX with a liquid lithium divertor module *Contrib. Plasma Phys.* **50** 368–73

[6] Raman R. *et al* and the NSTX Research Team 2001 Initial results from coaxial helicity injection experiments in NSTX *Plasma Phys. Control. Fusion* **43** 305–12

[7] Huang J.A. and Menard J. 2005 Development of an auto-convergent free-boundary axisymmetric equilibrium solver *American Physical Society, 47th Annual DPP Meeting (Denver, Colorado, 24–28 October 2005)* (New York: American Physical Society) *abstract GP1 045* http://meetings.aps.org/link/BAPS.2005.DPG.GP1.45

[8] Ferron J.R., Walker M.L., Lao L.L., St. John H.E., Humphreys D.A. and Leuer J.A. 1998 Real time equilibrium reconstruction for tokamak discharge control *Nucl. Fusion* **38** 1055–66

[9] Hagglund T. and Astrom K.J. 1995 *PID Controllers: Theory, Design, and Tuning* 2nd edn (Research Triangle Park, NC: Instrument Society of America)

[10] Penaflor B.G., Ferron J.R. and Walker M.L. 1996 A structured architecture for advanced plasma control experiments *Proc. 19th Symp. on Fusion Technology (Lisbon, Portugal) (16–20 September)* p 965

[11] Gates D.A. *et al* 2006 Progress towards steady state on NSTX *Nucl. Fusion* **46** S22–28

[12] Gates D.A. *et al* and the NSTX Research Team 2007 Progress towards steady state at low aspect ratio on the National Spherical Torus Experiment NSTX *Nucl. Fusion* **47** 1376–82

[13] Gopal M. 2003 *Digital Control and State Variable Methods, 2e: Conventional and Neuro-Fuzzy Control Systems Book* 2nd edn (New Delhi: Tata McGraw-Hill) p 164

[14] Xue D., Chen Y.Q. and Atherton D.P. 2008 *Linear Feedback Control: Analysis and Design with MATLAB (Advances in Design and Control)* (Philadelphia, PA: Society for Industrial and Applied Mathematics)

[15] Piras F. *et al* 2009 Snowflake divertor plasmas on TCV *Plasma Phys. Control. Fusion* **51** 055009

[16] Ryutov D.D. 2007 Geometrical properties of a 'snowflake' divertor *Phys. Plasmas* **14** 064502

[17] Ryutov D.D., Cohen R.H., Rognlien T.D. and Umansky M.V. 2008 The magnetic field structure of a snowflake divertor *Phys. Plasmas* **15** 092501